physica status solidi rrl
www.pss-rapid.com

Check for updates

Short Drying Processes for Silicon Solar Cells

Daniel Ourinson, Michael Linse, Markus Klawitter, and Andreas Lorenz*

Herein, very short drying processes for the screen-printed electrodes of passivated emitter and rear solar cells (PERC) are successfully demonstrated. The short drying processes are conducted in an in-line heating system with vertical-cavity surface-emitting lasers (VCSEL) as its heat source, being a compact alternative to the conventional heating chamber. While the heating time of the conventional industrial drying process is believed to be about 20 s (to the best of the authors' knowledge), the VCSEL system allows a significant reduction down to 0.15 s while maintaining a similar power conversion efficiency and contact adhesion quality.

1. Introduction

A general aim of the photovoltaic (PV) industry is to reduce process times to decrease the cycle time of a solar cell and increase the throughput.[1] This work focuses on reducing the process time of the contact drying step[2–4] (t_{DRY}) for high-temperature solar cell devices like passivated emitter and rear cells (PERC)[5–7] and tunnel oxide passivated contact (TOPCon) cells[8–13] while maintaining the level of the solar cell performance. The drying process is required after the screen-printing of metal pastes (electrodes) on the solar wafer substrate.[14–16] Most notably, the goals of the drying process are to evaporate the solvents of the paste, mitigate avoidable spreading of the paste, and ensure adhesion of the paste to the wafer substrate for subsequent handling and screen-printing processes. The industrial drying process is conducted in an in-line conveyor belt furnace with a heating chamber based on heating by infrared (IR) lamps and/or convective heating. To the best of the authors' knowledge, a corresponding industrial drying step is currently about 30 s long (20 s heating part ($t_{DRY\text{-}H}$), 10 s cooling part ($t_{DRY\text{-}C}$)), during which the solar cell is typically heated to a temperature of $T \approx 200$–250 °C. To achieve the reduction of t_{DRY}, an alternative compact in-line heating device compared to a conventional heating chamber is utilized. This alternative system features directional panel radiators, namely vertical-cavity surface-emitting lasers (VCSEL),[17–19] as its heat source (see **Figure 1**). This "VCSEL system" has already been conceptualized in Ref.[20] to demonstrate an alternative firing process. The VCSEL system is suitable to demonstrate short drying processes (further called "VCSEL drying") since the length of the illumination area in the transport direction on a passing solar cell is 5 cm (17 cm perpendicular to the transport direction), while the conveyor belt velocity ranges between $v_{BELT} = 1$–20 m min^{-1}, yielding $t_{DRY\text{-}H} = 0.15$–3 s, which is significantly shorter than the $t_{DRY\text{-}H}$ of the conventional drying process.

D. Ourinson, M. Linse, M. Klawitter, A. Lorenz
Photovoltaics
Production Technology - Structuring and Metallization
Fraunhofer Institute for Solar Energy Systems
Heidenhofstraße 2, 79110 Freiburg, Germany
E-mail: daniel.ourinson@ise.fraunhofer.de

The ORCID identification number(s) for the author(s) of this article can be found under https://doi.org/10.1002/pssr.202200149.

© 2022 The Authors. physica status solidi (RRL) Rapid Research Letters published by Wiley-VCH GmbH. This is an open access article under the terms of the Creative Commons Attribution-NonCommercial License, which permits use, distribution and reproduction in any medium, provided the original work is properly cited and is not used for commercial purposes.

DOI: 10.1002/pssr.202200149

2. Results and Discussion

Figure 2a shows that VCSEL-dried solar cells achieve the same power conversion efficiency (η) level as the conventionally dried solar cells (further I–V parameters listed in **Table 1**). More precisely, similar power conversion efficiencies are achieved for $t_{DRY\text{-}H}$ down to 1.5 s—without applying the "laser enhanced contact optimization" (LECO) process. The reduced power conversion efficiencies for shorter t_{DRY} stem mainly from series resistance losses, as can be obtained from the higher difference between the fill factor and pseudo-fill factor (pFF-FF) in Figure 2b. Meanwhile, the reduced power conversion efficiencies seem not to stem from the open-circuit voltage (V_{OC}) or the short-circuit current (j_{SC}), since the latter parameters do not vary significantly for the investigated experimental groups (see Table 1). After LECO treatment, the pFF-FF values are reduced (especially for samples undergoing very short $t_{DRY\text{-}H}$) and equalized to the same level for all sample groups. Since LECO improves underfired silver–silicon contacts to optimum level, this result suggests a critical t_{DRY} below which such contacts are underfired. This reduction of the series resistance losses leads to an improvement of the power conversion efficiency—especially for very short $t_{DRY\text{-}H}$—elevating the level to that of the conventional reference for all investigated sample groups, including the shortest $t_{DRY\text{-}H}$. Though, one can see a slight trend of power conversion efficiency reduction and deviation increase with shorter $t_{DRY\text{-}H}$, suggesting that even shorter $t_{DRY\text{-}H}$ would lead to further efficiency reduction.

When evaluating the $t_{DRY\text{-}C}$ of the VCSEL drying, as described in Section 2, **Figure 3** reveals that it takes about 5 s for a sample to cool from 225 to 25 °C under the prevailing conditions. Since the sample cooling to room temperature is necessary to proceed with the subsequent screen-printing step in the process chain, t_{DRY} is limited by $t_{DRY\text{-}C}$. Therefore, reducing $t_{DRY\text{-}H}$ with the goal to

© 2022 The Authors. physica status solidi (RRL) Rapid Research Letters published by Wiley-VCH GmbH

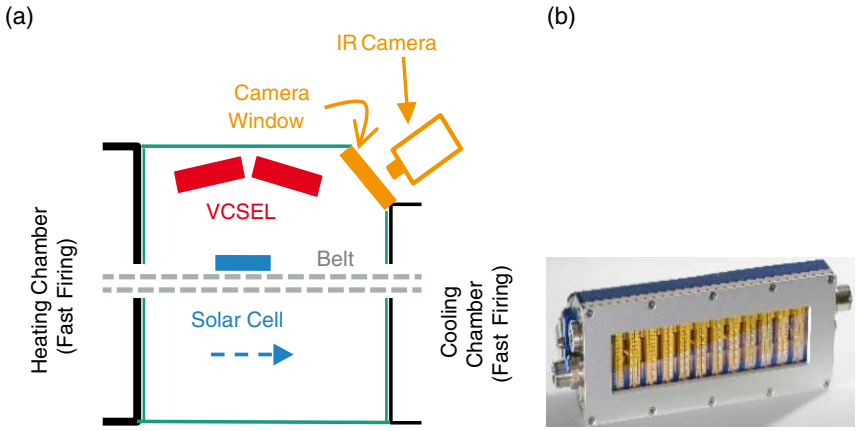

Figure 1. a) Scheme of the VCSEL-based heating chamber (adapted with permission Ref. [20], Copyright 2021, IEEE). The dashed blue arrow indicates the transport direction of the solar cells. b) Image of one of the utilized VCSEL modules (reproduced with permission Ref. [20], Copyright 2021, IEEE).

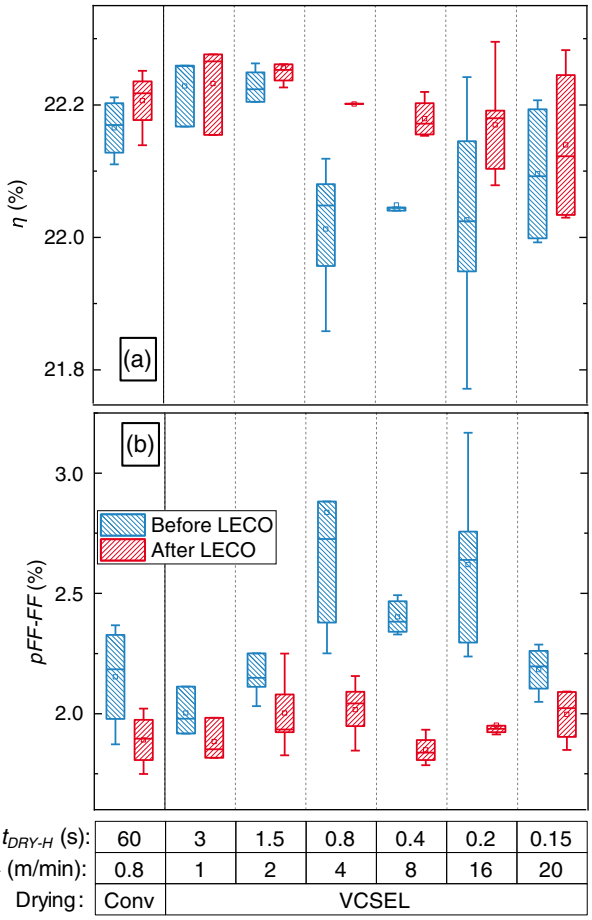

Figure 2. *I–V* results of the power conversion efficiency and *pFF-FF* values for all investigated sample groups in the present work. Abbreviations: Conv = conventional.

reduce t_{DRY} significantly becomes more and more insignificant with shorter t_{DRY-H}. For example, t_{DRY} seems not to shorten significantly when shortening t_{DRY-H} from 0.4 to 0.15 s, while $t_{DRY-C} = 5$ s since t_{DRY} is merely reduced from 5.4 to 5.15 s. Hence, in the authors' opinion, there is no need to investigate even shorter t_{DRY-H} then those already investigated in the present work. In the future, a potential further reduction of t_{DRY-C} should be investigated. Reducing the surrounding temperature could lead to a faster cooldown of the solar cell.

Figure 4 shows the results of the 90° peel tests after soldering, as described in Section 2. On the one hand, the adhesion tests reveal that the peel force is below the recommended value of 1 N mm^{-1} (corresponding to 0.9 N in Figure 4) for all investigated drying processes, including the conventional reference—for the front- and rear-side contact. On the other hand, these tests reveal that the shorter drying processes maintain a similar peel force level compared to the conventional reference for most of the sample groups (except for the rear contact featuring $t_{DRY-H} = 1.5$ s for unknown reasons). Thus, a shorter t_{DRY} using VCSEL drying does not seem to reduce the contact adhesion, indicating that the faster processes meet the requirements for module production. On that note, the utilized pastes themselves might lead to a lower adhesion than the recommended value of 1 N mm^{-1}.

3. Summary and Conclusion

This work successfully demonstrates very short drying processes for PERC devices. The short drying processes are conducted in an in-line alternative heating system with directional panel radiators, namely VCSEL modules, as its heat source. This VCSEL system is significantly more compact than a conventional drying furnace (approximately one-third of the device length in the case of the present work). Without utilizing the LECO process, similar power conversion efficiencies down to $t_{DRY-H} = 1.5$ s can be achieved with the "VCSEL drying" compared to the conventional drying in a classic in-line heating chamber. With the LECO process, similar power conversion efficiencies down to $t_{DRY-H} = 0.15$ s can be achieved. The addition of $t_{DRY-C} = 5$ s results in a total drying time of $t_{DRY} = 5.15$ s. This is a massive reduction compared to the believed conventional $t_{DRY} \approx 30$ s. Since $t_{DRY} = 5.15$ s is achieved with $v_{BELT} = 20$ m min^{-1}—being nearly twice as fast as in the industrial

© 2022 The Authors. physica status solidi (RRL) Rapid Research Letters published by Wiley-VCH GmbH

18626270, 2022, 8, Downloaded from https://onlinelibrary.wiley.com/doi/10.1002/pssr.202200149 by Fraunhofer Ise Inst. Solar Energy Systems, Wiley Online Library on [17/04/2023]. See the Terms and Conditions (https://onlinelibrary.wiley.com/terms-and-conditions) on Wiley Online Library for rules of use; OA articles are governed by the applicable Creative Commons License

Table 1. Additional *I–V* results to those of Figure 2, namely the open-circuit voltage (V_{OC}), short-circuit current (j_{SC}), and fill factor (FF) for all investigated sample groups in the present work after LECO treatment. The values display average and standard deviation per group.

Drying:	Conventional	VCSEL	VCSEL	VCSEL	VCSEL	VCSEL	VCSEL
t_{DRY_H} [s]	60	3	1.5	0.8	0.4	0.2	0.15
V_{OC} [mV]	677 ± 0.5	678 ± 1.0	679 ± 0.7	678 ± 1.1	679 ± 0.5	678 ± 0.6	678 ± 1.5
j_{SC} [mA cm^{-2}]	40.2 ± 0.1	40.2 ± 0.1	40.2 ± 0.1	40.2 ± 0.1	40.1 ± 0.1	40.1 ± 0.1	40.1 ± 0.1
FF [%]	81.6 ± 0.1	81.5 ± 0.1	81.6 ± 0.1	81.5 ± 0.1	81.6 ± 0.1	81.5 ± 0.1	81.5 ± 0.2

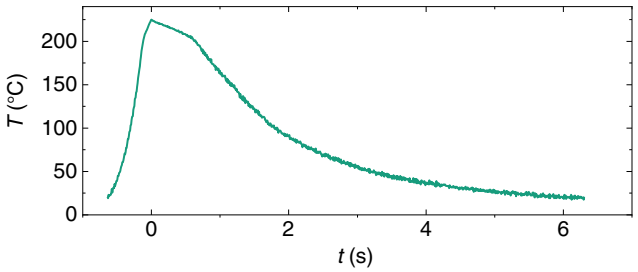

Figure 3. Resulting time–temperature profile after static VCSEL heating with the goal to estimate $t_{DRY\text{-}C}$ in the case of VCSEL drying (see experimental section).

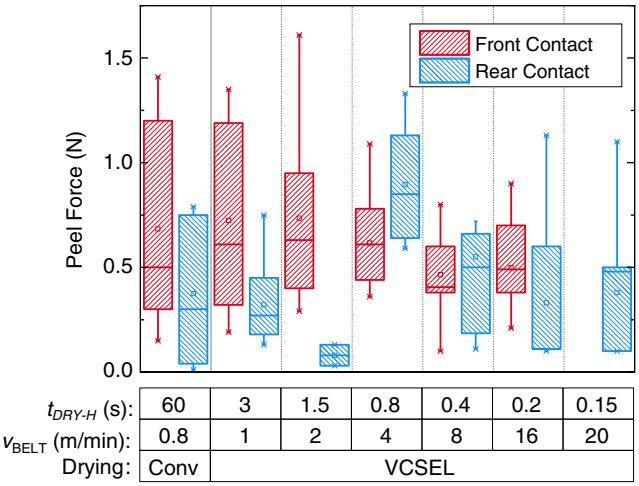

Figure 4. Results of the adhesion tests for all investigated sample groups in the present work. Unfortunately, no useful data could be retrieved for the front contact featuring $t_{DRY\text{-}H} = 0.15$ s.

PV production (to the best of the authors' knowledge)—the VCSEL system demonstrates a significantly higher throughput for the drying step. Adhesion tests suggest no reduction of contact adhesion (both front and rear side) due to a shorter t_{DRY}, indicating module compatibility for corresponding solar cells.

4. Experimental Section

This work is demonstrated on industrial M2-sized *p*-type monofacial PERC devices, representatively for all industrial high-temperature solar cells, including bifacial and TOPCon solar cells. The main process flow of this work is visualized in **Figure 5**.

In an industrial process chain, there are typically up to four screen-printing steps: rear-side silver pads, rear-side full-area aluminum, front-side silver fingers, and front-side silver busbars (being the "dual print" version on the front side). There are three drying steps between the screen-printing steps, which demonstrates the relevance to reduce t_{DRY}. The drying after the last screen-printing step is combined with the firing step. Compared to the earlier-mentioned scenario, the present work features only three screen-printing steps: the front-side dual print is combined to a single print, depositing a silver H-pattern grid. But there are three drying steps because the drying after the front-side screen-printing step (being the last screen-printing step) is separated from the firing step. To a certain extent, the latter drying step is similar to the drying step after the first front-side screen-printing step in the dual-print scenario.

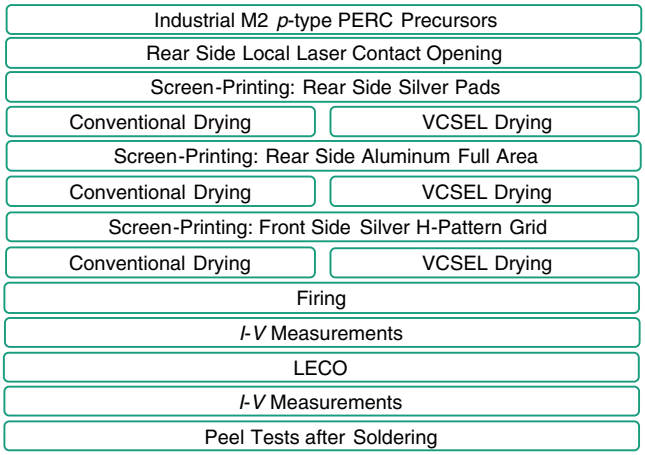

Figure 5. Main process flow of the present work.

Each sample group contains five samples. A reference sample group featuring conventional drying is present. Contrary to the believed industrial t_{DRY}, the conventional drying furnace at the authors' institution features $t_{DRY} = 90$ s—with $t_{DRY\text{-}H} = 60$ s and $t_{DRY\text{-}C} = 30$ s. For all the other sample groups, the drying step is conducted by the VCSEL system. The latter features two 160 × 40 mm VCSEL modules with 808 nm wavelength and 9.6 kW combined power, resulting in power densities of about 100 W cm^{-2} on the passing solar cell. A horizontal air knife is installed below the VCSEL modules to prevent the volatile organics evaporated from the pastes to deposit on the modules. The length of the VCSEL chamber in transport direction amounts to 80 cm, while the used conventional drying furnace is 230 cm long, making the VCSEL system significantly more compact. The temperature during the VCSEL drying is monitored via IR thermography,[21] as visualized in Figure 1a. Preliminary tests have revealed that the optimum solar cell temperatures for VCSEL drying are similar to those for conventional drying, namely 170–270 °C—being valid for all three types of the applied metallization steps. Due to its configuration, the VCSEL system causes a relatively inhomogeneous temperature distribution over the whole solar cell area, as explained in Ref. [20]. **Figure 6** shows a representative temperature distribution during the VCSEL drying, having a span of about 70 K (representative regarding v_{BELT} and drying step). To stay within the optimum temperature range, the average temperature is kept at 225 °C for all sample groups throughout this work. As indicated in Section 1, the v_{BELT} of the VCSEL system is varied,

© 2022 The Authors. physica status solidi (RRL) Rapid Research Letters published by Wiley-VCH GmbH

18626270, 2022, 8, Downloaded from https://onlinelibrary.wiley.com/doi/10.1002/pssr.202200149 by Fraunhofer Ise Inst. Solar Energy Systems, Wiley Online Library on [17/04/2023]. See the Terms and Conditions (https://onlinelibrary.wiley.com/terms-and-conditions) on Wiley Online Library for rules of use; OA articles are governed by the applicable Creative Commons License

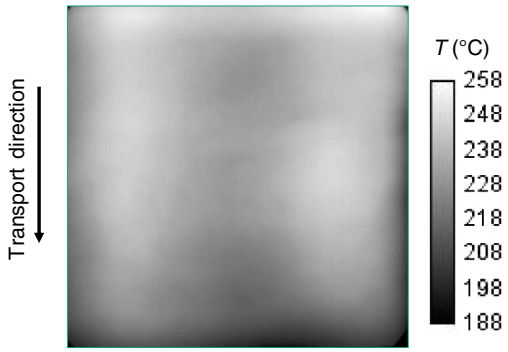

Figure 6. Spatial temperature distribution of a solar cell during the VCSEL drying of the rear-side full-area aluminum layer at $v_{BELT} = 2\ m\ min^{-1}$.

namely from 1 to 20 m min^{-1}, leading to different $t_{DRY\text{-}H}$. Please note that a chosen v_{BELT} applies for all three drying steps of the respective sample.

In this work, it is important to distinguish between $t_{DRY\text{-}H}$ and $t_{DRY\text{-}C}$, since only the heating part of the VCSEL drying can be monitored with the IR camera, while the cooling part is out of its field of view. However, it is important to know $t_{DRY\text{-}C}$, because the solar cell must be cooled to room temperature in order to proceed with the next screen-printing step. Unfortunately, thermocouple measurements cannot be conducted in the VCSEL chamber, as explained in Ref. [20]. $t_{DRY\text{-}C}$ is negligibly influenced by v_{BELT} but significantly by the difference of the temperature of the solar cell and its surrounding. Since the surrounding temperature in the laser chamber is more or less constant, it is justified in the opinion of the authors to use the following method to estimate $t_{DRY\text{-}C}$ during VCSEL drying: a solar cell is statically ($v_{BELT} = 0$) heated by the VCSEL modules to 225 °C and subsequently cooled down to room temperature (utilization of active cooling). Since the solar cell is not moving, the time–temperature curve can be recorded by the IR camera in this case.

After firing, the solar cells are *I–V* measured, obtaining among others the values of η, V_{OC}, j_{SC}, FF, and pFF. The V_{OC} is taken as a measure for recombination.[22] The j_{SC} is taken as a measure for charge carrier generation quality.[22] The difference between pFF and FF is taken as a measure for series resistance losses.[23] The power conversion efficiency is taken as a measure for the overall solar cell performance. After the initial *I–V* measurements, the solar cells are treated with the LECO process[24–28] and *I–V* measured again. LECO is a relatively new process that improves underfired silver–silicon contacts to the optimum stage and is, therefore, more and more used in the PV community. Reducing $t_{DRY\text{-}H}$ can potentially cause bad adhesion of the contacts. For this reason, adhesion tests after IR soldering according to the standard DIN EN 50 461 are conducted for two samples per side for each drying profile.[29]

Acknowledgements

This work was supported in part by the German Federal Ministry for Economic Affairs and Climate Action within the research project "Rock-It" under Grant 0324306B. The authors would like to thank Mohammad Abazid, Sonja Faller, Maxim Kümmerle, and all the colleagues who contributed to this work.

Open Access funding enabled and organized by Projekt DEAL.

Conflict of Interest

The authors declare no conflict of interest.

Data Availability Statement

The data that support the findings of this study are available from the corresponding author upon reasonable request.

Keywords

drying, passivated emitter and rear solar cells (PERC), process time, throughput, vertical-cavity surface-emitting lasers (VCSEL)

Received: April 26, 2022
Revised: June 3, 2022
Published online: July 6, 2022

[1] VDMA, *Inter. Technology Roadmap for Photovoltaic (ITRPV)*, **2021**.
[2] T. Dullweber, *Silicon Solar Cell Metallization and Module Technology*, Institution of Engineering & Technology, Stevenage **2021**.
[3] E. Sowade, H. Kang, K. Y. Mitra, O. J. Weiß, J. Weber, R. R. Baumann, *J. Mater. Chem. C.* **2015**, *3*, 11815.
[4] I. B. Cooper, A. Ebong, J. S. Renshaw, R. Reedy, M. Al-Jassim, A. Rohatgi, *IEEE Electron Device Lett.* **2010**, *31*, 461.
[5] A. W. Blakers, A. Wang, A. M. Milne, J. Zhao, M. A. Green, *Appl. Phys. Lett.* **1989**, *55*, 1363.
[6] T. Dullweber, C. Kranz, R. Peibst, U. Baumann, H. Hannebauer, A. Fülle, S. Steckemetz, T. Weber, M. Kutzer, M. Müller, G. Fischer, P. Palinginis, H. Neuhaus, *Prog. Photovolt: Res. Appl.* **2016**, *24*, 1487.
[7] T. Dullweber, J. Schmidt, *IEEE J. Photovolt.* **2016**, *6*, 1366.
[8] F. Feldmann, M. Bivour, C. Reichel, H. Steinkemper, M. Hermle, S. W. Glunz, *Sol. Energy Mater. Sol. Cells* **2014**, *131*, 46.
[9] Y. Chen, D. Chen, C. Liu, Z. Wang, Y. Zou, Y. He, Y. Wang, L. Yuan, J. Gong, W. Lin, X. Zhang, Y. Yang, H. Shen, Z. Feng, P. P. Altermatt, P. J. Verlinden, *Prog. Photovolt. Res. Appl.* **2019**, *27*, 827.
[10] A. Ingenito, C. Allebé, G. Nogay, J. Horzel, P. Wyss, J. A. Stückelberger, M. Despeisse, F-. Haug, C. Ballif, *A Passivating Contact Concept Compatible with a Short Thermal Treatment*, IEEE, Piscataway, NJ **2018**, p. 1524.
[11] D. K. Ghosh, S. Bose, G. Das, S. Acharyya, A. Nandi, S. Mukhopadhyay, A. Sengupta, *Surf. Interfaces* **2022**, *30*, 101917.
[12] D. Chen, Y. Chen, Z. Wang, J. Gong, C. Liu, Y. Zou, Y. He, Y. Wang, L. Yuan, W. Lin, R. Xia, L. Yin, X. Zhang, G. Xu, Y. Yang, H. Shen, Z. Feng, P. P. Altermatt, P. J. Verlinden, *Sol. Energy Mater. Sol. Cells* **2020**, *206*, 110258.
[13] A. Blakers, *IEEE J. Photovolt.* **2019**, *9*, 629.
[14] J. Xu, J. Zhang, K. Kuang, in *Conveyor Belt Furnace Thermal Processing*, Springer, Heidelberg **2018**.
[15] A. A. Wereszczak, M. C. Modugno, B. R. Chen, W. M. Carty, *IEEE Trans. Compon. Packag. Manufact. Technol.* **2017**, *7*, 2079.
[16] E. K. Sahni, B. Chaudhuri, *Int. J. Pharmaceut.* **2012**, *434*, 334.
[17] A. Pruijmboom, R. Apetz, R. Conrads, C. Deppe, G. Derra, S. Gronenborn, X. Gu, J. S. Kolb, M. Miller, H. Moench, F. Ogiewa, P. Pekarski, J. Pollmann-Retsch, U. Weichmann *Proc. SPIE.*, **2016**, *28*, 032005.
[18] VCSEL *Solutions & photodiodes TRUMPF*, https://www.trumpf.com/en_US/products/vcsel-solutions-photodiodes/, (accessed: January, 2020).
[19] A. Pruijmboom, *Laser Focus World.* **2014**.
[20] D. Ourinson, G. Emanuel, K. Rahmanpour, F. Ogiewa, H. Muller, E. Krassowski, H. Hoffler, F. Clement, S. W. Glunz, *IEEE J. Photovolt.* **2021**, *11*, 282.
[21] D. Ourinson, G. Emanuel, A. Csordás, G. Dammaß, H. Müller, C. Sternkiker, F. Clement, S. W. Glunz, *Phys. Status Solidi RRL* **2019**, *13*, 1900270.
[22] J. Greulich, M. Glatthaar, A. Krieg, G. Emanuel, S. Rein, in *24th EuPVSEC.* **2009**.
[23] J. Greulich, M. Glatthaar, S. Rein, *Prog. Photovolt: Res. Appl.* **2010**, *18*, 511.

© 2022 The Authors. physica status solidi (RRL) Rapid Research Letters published by Wiley-VCH GmbH

18626270, 2022, 8, Downloaded from https://onlinelibrary.wiley.com/doi/10.1002/pssr.202200149 by Fraunhofer Ise Inst. Solar Energy Systems, Wiley Online Library on [17/04/2023]. See the Terms and Conditions (https://onlinelibrary.wiley.com/terms-and-conditions) on Wiley Online Library for rules of use; OA articles are governed by the applicable Creative Commons License

[24] E. Krassowski, S. Großer, M. Turek, H. Höffler, in *37th Photovoltaic Conf. Proc., Online-Conf.* **2020**.
[25] R. Mayberry, K. Myers, V. Chandrasekaran, A. Henning, H. Zhao, E. Hofmüller, *36th Photovoltaic Conf. Proc., Marseille, France* **2019**.
[26] E. Krassowski, B. Jaeckel, U. Zeller, M. Pander, P. Schenk, E. Hofmueller, H. Hanifi, *Sol. RRL.* **2021**, 2100537.
[27] S. Groser, E. Krassowski, S. Swatek, H. Zhao, C. Hagendorf, *IEEE J. Photovolt.* **2022**, *12*, 26.
[28] E. Krassowski, S. Großer, M. Turek, A. Henning, H. Zhao, *AIP Conf. Proc.* **2021**, *2367*, 20005.
[29] *Solarzellen - Datenblattangaben und Angaben zum Produkt für kristalline Silicium-Solarzellen (DIN EN 50461:2007-03)*, Deutsches Institut für Normung e.V **2007**.

© 2022 The Authors. physica status solidi (RRL) Rapid Research Letters published by Wiley-VCH GmbH

18626270, 2022, 8, Downloaded from https://onlinelibrary.wiley.com/doi/10.1002/pssr.202200149 by Fraunhofer Ise Inst. Solar Energy Systems, Wiley Online Library on [17/04/2023]. See the Terms and Conditions (https://onlinelibrary.wiley.com/terms-and-conditions) on Wiley Online Library for rules of use; OA articles are governed by the applicable Creative Commons License